

The Terrestrial Magnetospheric Response to the 28th October 2021 CME

J. E. Waters¹, C. M. Jackman², D. K. Whiter¹, A. R. Fogg², L. Lamy^{3,4}, J.
Carter⁵, L. Fryer¹, C. Louis², E. Carley², C. Briand³, K. Issautier³, L.
Paxton⁶, B. Cecconi³, X. Bonnin³, P. Gallagher²

¹Space Environment Physics Group, School of Physics and Astronomy, University of Southampton,
Southampton, UK

²School of Cosmic Physics, DIAS Dunsink Observatory, Dublin Institute for Advanced Studies, Dublin 15,
Ireland

³LESIA, Observatoire de Paris, PSL Research University, CNRS, Sorbonne Université, Univ. Paris,
Meudon, France

⁴LAM, Pythéas, Aix Marseille Université, CNRS, CNES, 38 Rue Frédéric Joliot Curie, 13013 Marseille,
France

⁵Radio and Space Plasma Physics Group, Physics and Astronomy, University of Leicester, Leicester, UK
⁶Applied Physics Laboratory, John Hopkins University, Laurel, Maryland, USA

Key Points:

- OMNI data upstream of Earth reveal the effects of the arrival of a CME at the bowshock
- SuperMAG SML indices suggest multiple substorm onsets during an energised ring current in response to the CME
- Novel Wind observations of AKR from L1 are likely generated above bright, discrete auroral structures between 14:00-18:00 MLT, observed by SSUSI

Corresponding author: James Waters, J.Waters@soton.ac.uk

Abstract

On October 28th 2021 the Sun released a large Coronal Mass Ejection (CME) in Earth's direction. An X1.0 class solar flare and a rare ground level enhancement (GLE) were observed, along with bright solar radio bursts. Here we examine data from the near-Earth environment to investigate the terrestrial response to this solar event, as a typical example of Sun-Earth interactions. The CME arrival is tracked at ~ 1 AU from Wind radio observations and the interplanetary magnetic field (IMF) and solar wind dynamic pressure by *in-situ* measurements of OMNI spacecraft. Geomagnetic activity is studied with indices including SYM-H while the auroral response is monitored by remote Wind radio measurements of Auroral Kilometric Radiation (AKR) and SSUSI UV observations. We quantify the timeline for solar wind-magnetosphere coupling via exploration of the dayside reconnection rate and polar cap voltages and address the visibility of AKR sources for a dayside radio observatory.

Plain Language Summary

The Sun can emit Coronal Mass Ejections (CME), which are energetic releases of plasma that travel through the solar system at high speeds. This outflow of mass has a significant effect on the terrestrial magnetosphere, and produces space weather effects at Earth under certain conditions. A CME occurred on 28th October 2021 that was directed towards Earth, and observable signatures were monitored upstream. This study presents the observations of the CME arrival at Earth, as well as the response of the terrestrial magnetosphere using various proxy indices of geomagnetic activity and novel observations of Auroral Kilometric Radiation far from Earth on the dayside.

1 Introduction

A partially Earth-directed CME was observed at 15:35 UT on 2021 October 28th, following an X1.0 class solar flare emitted from the AR12887 region and the ejection of relativistic protons and electrons from the solar atmosphere. The solar protons (~ 450 MeV) produced rare ground level enhancements (GLEs) at Earth, one of five since 1976 that occurred with a flare of this magnitude (Papaioannou et al., 2022). Accelerated electrons radiated non-thermal radio emission in a host of particularly intense solar radio type II, III and IV bursts (Klein et al., in prep., 2022). The CME was observed by the Large Angle Spectrometric Coronagraph (LASCO; (Brueckner et al., 1995)) C2 as a partial halo propagating towards the south. From the broader literature (e.g., Taylor et al., 1994; Hutchinson et al., 2011; Kilpua et al., 2017), we expect a strong geomagnetic response when the upstream medium is characterized by high solar wind flow speed, high solar wind dynamic pressure and southward-directed interplanetary magnetic field (IMF).

This solar activity provided an opportune event, in the new rising phase of the solar cycle, to study its effect on Earth's magnetosphere in the space weather context. While *in-situ* observations can provide insight into the solar wind plasma itself, the suite of terrestrial instruments (both remote and ground-based) can also be used to track the coupling of the magnetosphere to the CME-associated solar wind. With upstream monitors like Wind at the Lagrange point L1, the interplanetary magnetic field (IMF) and plasma parameters can be measured continuously. These parameters have been used to define non-linear coupling relationships (e.g., Milan et al., 2012) that characterize magnetic reconnection processes between the IMF and the planetary magnetic field on the dayside of the terrestrial magnetosphere, allowing inference of open flux being transported across the polar cap and into the nightside magnetosphere. Widely distributed magnetometer stations are used to measure the magnetic disturbance, signalling strengthened current systems and the onset of storms and substorms (Iyemori, 1990; Newell & Gjerloev, 2011). Electron precipitation along magnetic field aligned currents (FACs) produces the UV and optical aurora in the ionosphere, but also source regions of Auroral Kilometric Radia-

tion (AKR) above it under certain conditions (e.g., Wu & Lee, 1979; Treumann, 2006). These auroral emissions, monitored remotely, provide a comprehensive picture of the dynamics of the auroral acceleration region when accounting for complex viewing effects of AKR (Gurnett, 1974; Alexander & Kaiser, 1976; Mutel et al., 2008; Zhao et al., 2019).

In this study, we examine the response of the near-Earth environment in terms of solar wind conditions and various geomagnetic indices, giving both an in-situ and remotely sensed picture of magnetospheric conditions in the days during and following the arrival of the CME. Furthermore, we present subsequent, novel observations of AKR made by Wind/Waves from L1, 250 R_E from Earth. Section 2 presents the observations made throughout the coupling timeline following the CME: Section 2.1 describes the upstream solar wind conditions following the arrival of the ICME at Earth. Section 2.2 describes the timeline of the geomagnetic response at various scales using OMNI data, SuperMAG geomagnetic indices (Gjerloev, 2012) and PC indices (Stauning, 2013), supplemented by Wind/WAVES AKR observations. Section 2.3 presents UV auroral observations with the observed AKR to interpret the driving origin of the radio emission. Section 3 summarises the case study of the event.

2 Observations

2.1 Solar Wind Conditions at the Bowshock

Figure 1 shows a combination of remote sensing and *in-situ* data which illustrate the impact of the CME at Earth. Radio observations made by the Wind/WAVES/RAD1 instrument are seen in the top panel, exhibiting clear signatures of solar type III radio bursts, characterised by bright sweeping arcs that are much more intense than the radio background. Type IIIs are generated by fast ($\sim 0.3c$) electron beams; in this instance electrons were estimated to have energies of 9 keV and a travel time of 1 hour between the solar corona and Wind (Klein et al., in prep., 2022). Their arrival is seen in panel a of Figure 1. Accounting for the ~ 8 minute light travel time from the Sun, the intense solar type III storm at $\sim 15:30$ thus indicates the time of the eruption of the CME from the solar corona. The Langmuir waves, low frequency excitations at $\sim 18:00$ UT are the result of the Wind spacecraft travelling through the type III-producing electron beam, and as such a direct magnetic connection to the solar surface (Klein et al., in prep., 2022). Panels b and c illustrate the IMF and solar wind conditions as the CME sweeps over OMNI spacecraft, parked at the Lagrange 1 point 250 R_E upstream of Earth.

The Z and Y components of the interplanetary magnetic field (IMF) propagated to the terrestrial bow shock are presented in the panel b of Figure 1. At the beginning of the presented interval, the magnitude of both components is close to zero, often with weakly positive B_Z and weakly negative B_Y . While the total magnetic field begins to slowly increase from the start of the interval, significant fluctuations in the B_Z and B_Y IMF components and a total increase are seen from $\sim 21:00$ UT on 29th October 2021, after which large excursions in the Z and Y components continue as does the increase in the total magnetic field density. This results in a rotation in the clock angle, which is particularly dramatic at around 20:00 UT 30th October 2021, and continues afterwards. This is similar to signatures associated with the passing of an interplanetary coronal mass ejection (ICME) (e.g., Carter et al., 2020).

The solar wind characteristics during this event are presented in panel c of Figure 1, with the dynamic pressure in black, proton density in blue and flow speed in gold. Simultaneous to rotation in the clock angle mentioned previously, a multi-step increase in solar wind dynamic pressure is observed in the later half of 30th October 2021. The peak dynamic pressure of ~ 12 nPa occurs at 18:56. This pressure (proportional to $N_{SW}V_{SW}^2$) increase is dominated by the shape of the density curve displayed in blue, and no clear related signatures are observed in the flow speed for 30th October 2021. Combined with

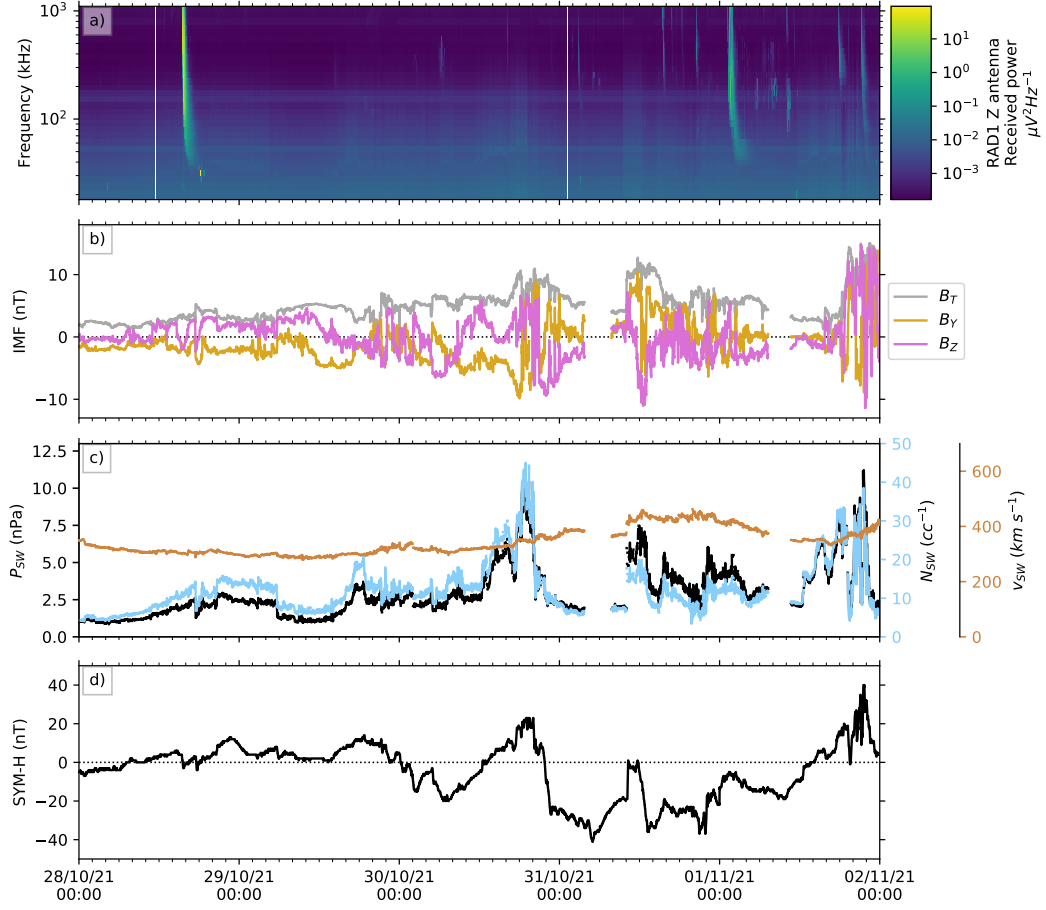


Figure 1. Observations between the 28th October and 2nd November 2021 of: a) radio emission showing intense Type III bursts near the time of the CME; b) total (B_T) and transverse (B_Y , B_Z) IMF magnitudes; c) solar wind flow pressure (P_{SW}), proton density (N_{SW}) and flow speed (V_{SW}); d) SYM-H, showing the terrestrial ring current response.

the clock angle rotation, this is indicative of the passing of an ICME, such as that observed by Carter et al. (2020). Noting that median P_{SW} values at 1 AU are of the order of several nPa (e.g., Fogg et al., 2022), a pressure enhancement reaching the order of 10 nPa suggests a substantially compressed magnetosphere. This is confirmed (Araki, 1994) by a rapid increase in SYM-H (presented in the panel d of the Figure 1), followed by a sharp decrease to negative values, with oscillations around the negative peak at $\sim 05:00$ UT, 31st October 2021. Such a signature, driven by a rapid compression of the magnetosphere, is known as a geomagnetic sudden storm commencement (SSC); shown to be driven by CMEs by Taylor et al. (1994). A disturbed recovery period is observed in SYM-H. This is an SSC of only moderate magnitude, surpassing the quiet level of -15 nT defined by Walach and Grocott (2019) by about 25 nT at the peak of the storm.

2.2 Geomagnetic Activity

Geomagnetic indices are powerful tools which characterise the state of the magnetosphere. In this study, SYM-H, PC(N,S), SMU and SML indices are used; all continuous, minute resolution products derived from ground based magnetometer data, thus not limited by spacecraft position. Each index is amalgamated from individual stations, and shows deflections in the magnetic field as a result of changes in overhead currents. SYM-H (Iyemori, 1990) is derived from magnetometers at equatorial latitudes, indicating changes in the ring current and showing characteristic signatures of geomagnetic storms (e.g., Walach & Grocott, 2019). The polar cap indices PC(N,S) (e.g. Troshichev & Andrezen, 1985; Stauning, 2013) are measured by stations at polar latitudes in the northern and southern (geographic) hemispheres; they record the strength of cross polar currents, with larger values suggesting faster antisunward flux transport. Finally, SMU and SML (Gjerloev, 2012) are the upper and lower envelopes of the SuperMAG electrojet index, and show the strength of the eastward and westward electrojets respectively. These are measured from magnetometers in the auroral zone, and are roughly equivalent to the auroral electrojet indices AU and AL (Davis & Sugiura, 1966), which were not available for this interval. Most famously, SML/AL show distinct substorm signatures (e.g., Newell & Gjerloev, 2011; Forsyth et al., 2015). Figure 2 shows several parameters which reveal the terrestrial magnetospheric response to the arrival of the CME.

Figure 2a shows the dayside reconnection rate of Milan et al. (2012) (equation 15), a method of representing the energy input from the solar wind at the magnetopause boundary. This represents the non-linear coupling effects that can stimulate a cycle of magnetospheric dynamics and precede other phenomena within the inner magnetosphere. The reconnection voltage increases with the variations in the transverse (Y and Z) components of the IMF, and gradual increase in solar wind speed, towards the end of 30th October 2021. The largest increase in the reconnection rate for this interval comes with the most extreme Southward IMF at midday on 31st October 2021.

Towards the beginning of the presented interval, the polar cap indices PC(N,S) are relatively quiet; PC(N) is around the median values presented by Fogg et al. (2022). Throughout the interval shown in Figure 2b, both PC(N) and PC(S) follow similar shapes, suggesting balanced flux transport in both hemispheres. At the start of 30th October 2021, around 07:00 UT, the PC indices exceed 4 mVm^{-1} , in a short lived enhancement, prior to the primary P_{SW} enhancement. The PC(N) index peaks at $\sim 5.0 \text{ mVm}^{-1}$ at 06:46 while PC(S) peaks at $\sim 4.1 \text{ mVm}^{-1}$ at 07:03. A subsequent enhancement is seen roughly within the main phase of the SSC, with corresponding oscillatory activity. Following this, more short-lived enhancements in the PC index are observed within the disturbed recovery period of the storm, including another minor negative deviation that could be indicative of further ring current energisation. The enhancements to the PC index that follow the initial pressure pulse, while shorter, reach similar values in PC(S) and slightly smaller (within $\sim 5\text{-}20\%$) values for PC(N). These enhancements evidence periods of rapid

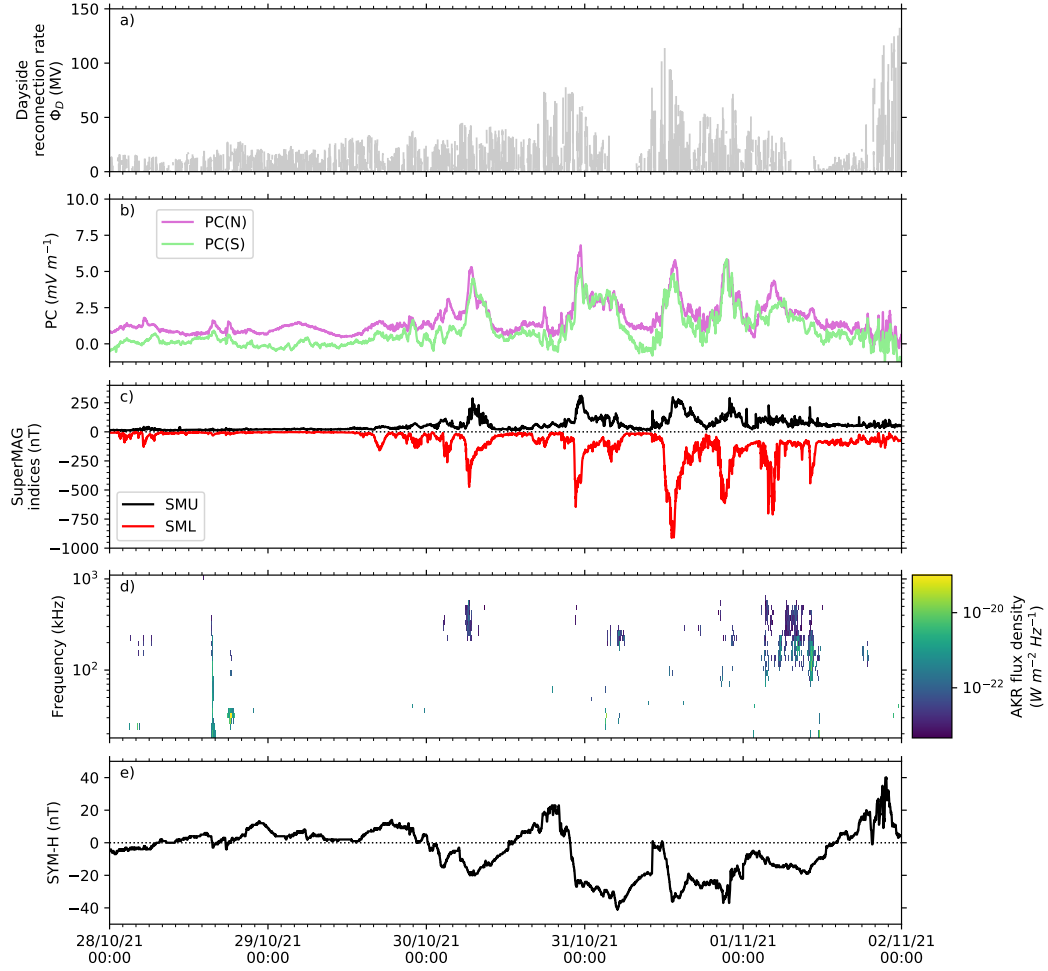


Figure 2. Magnetospheric response given by a) the dayside reconnection rate, b) PC indices for both hemispheres, c) auroral electrojet (SMU/SML) indices from SuperMAG, d) AKR observations made from L1 and e) the SYM-H index for 28th October to 2nd November 2021.

flux transport that facilitate the loading of magnetic energy; a prerequisite for the substorm dynamics of Figure 2c.

For all of the major SML diversions in the interval, their peak magnitude is at least two times greater than that of the SMU index, indicating a substorm-like response in the magnetosphere. The SMU and SML indices are both quiet at the beginning of the interval; SML reaching no more than -200 nT before 30th October 2021. A significant diversion in SML of -500 nT is seen at the same time as the first major increase of both PC indices on 30th October 2021; around 39 hours after solar flares associated with the 28th October 2021 CME were recorded. This diversion in the SML coincides with a Southward-turning IMF B_Z component, as seen in both Figure 1b and Figure 2a. Another significant SML peak is seen at $\sim 22:30$ UT, corresponding to the largest values of the day-side reconnection voltage since the arrival of the large pressure pulse as seen in Figure 1. This substorm onset accompanies the geomagnetic storm-like response of the SYM-H index, with the peak SML diversion occurring as SYM-H becomes negative.

The following substorm onset at $\sim 13:00$ UT, 31st October 2021, exhibits the largest disturbance to the geomagnetic field, with a negative peak of almost -1000 nT preceded (~ 30 min) by the peak dayside reconnection rate. The PC indices are lower than for the previous onset although peak in both hemispheres at ~ 5 mV m^{-1} . This onset also corresponds with a second pressure pulse in the solar wind and a second energisation of the ring current as shown by SYM-H. Another substorm onset occurs at $\sim 21:00$ UT, with a SML diversion of -600 nT, PC indices of similar values to the previous onset and during increased solar wind speed.

For 1st November 2021, a substorm onset is observed after the dayside reconnection rate decreases from 50 MV. SML values exhibit the second largest diversion of the interval; peaking close to -750 nT. The corresponding peaks in the PC indices exhibit asymmetry; the PC(S) index falls to nearly half of its original value at ~ 2.5 mV m^{-1} , while the PC(N) index falls to ~ 4 mV m^{-1} . While the SML profile around 04:00 UT contains the largest diversion for the 1st November 2021, smaller fluctuations occur until another questionable, smaller onset is seen at 10:00 UT. These high latitude current fluctuations occur while the ring current is recovering from storm-time conditions on average, although the SYM-H behaviour local to 04:00 UT is again decreasing, suggesting a minor introduction of solar wind particles.

When comparing SML values for time periods identified as substorm onset by various observational signatures, Forsyth et al. (2015) found the largest of the median SML diversion was -200 nT, for the event list of Newell and Gjerloev (2011). Coxon et al. (2014) found that typical substorms have an average SML disturbance of -400 nT. Although “supersubstorms” can produce diversions of -2700 nT (Nishimura et al., 2020), this implies that the substorm onsets seen during this interval are large compared to phenomena typically classified as a substorm.

Figures 2d and 2e also show observations that serve as a proxy for the geomagnetic response, albeit on different scales. The following Section 2.3 accounts for the AKR observations of Figure 2d and attempts to infer dayside magnetospheric dynamics via conjugate auroral observations. The aforementioned SYM-H in Figure 2e is described in Section 2.1.

2.3 AKR and Dayside Aurora

Figure 2d shows observations of AKR from Wind/WAVES/RAD1 following application of the process described in J. E. Waters et al. (2021). The Wind spacecraft was located at L1 during the entire interval. As AKR source regions are usually found on the nightside and the beaming is highly directed, Wind cannot readily observe AKR from substorm-associated auroral dynamics while it is at L1 (Mutel et al., 2008; J. E. Waters

et al., 2021; Fogg et al., 2022). Previous observations have also revealed AKR sources more widely distributed in the dusk and even dayside sectors (Mutel et al., 2008), as well as other mechanisms for dayside sources such as cusp aurora and transpolar arcs (e.g., Alexander & Kaiser, 1977; Pedersen et al., 1992; Hanasz et al., 2000; Mutel et al., 2004). Although some emission retained by the selection here is sparse at typical AKR frequencies (100-700 kHz (Morioka et al., 2007, 2013)), sometimes observed to occur for the time of a single frequency sweep (3 minutes), there are also periods of longer, continuous bursts. Intense emission at low frequencies, ~ 30 kHz at $\sim 18:00$ on 28th October 2021, is due to excited electrons in local plasma at the arrival of the solar type III electron beam at the instrument (Klein et al., 2022), and not AKR.

Sustained AKR bursts are seen after 30th October 2021, the most prominent just before 06:00 UT, lasting 2 hours between 250-500 kHz and for a 9 hour period from $\sim 03:00$ UT on 1st November 2021. The latter, most significant observations of AKR are seen on 1st November 2021; emission is observed from 03:00 to 11:00 UT between ~ 80 -500 kHz and is the most intense in this interval. Bursts of emission between 80-150 kHz are more intense than other AKR observed on this date, and exhibit apparent periodicity of ~ 2 hours. Fainter AKR is observed at higher frequencies (150-500 kHz).

Each observed AKR burst coincides with an SML diversion < -250 nT. However, some of the intervals of largest SML diversion see no AKR observations. Notably, substorm onsets at 22:15 UT on 30th October and 13:00 UT on 31st October are not accompanied by significant AKR observations. While short, sporadic AKR observations are made on the 31st October, they are minor considering this is the largest substorm onset observed for the period. Observations on the 1st November are similar, with the more sustained (30-60 min), apparently periodic bursts of AKR following substorm onset.

While sources of AKR production on the dayside magnetosphere do exist, it is difficult to discern these from AKR observations and accompanying geomagnetic indices directly, due to the differing scale of the associated plasma dynamics. While it cannot be assumed that L1 observations represent the entirety of the global AKR spectrum, it is also true that the lack of AKR does not immediately imply its absence due to the aforementioned viewing constraints. As well as dayside sources of AKR, illumination of Wind/WAVES by AKR sources could be due to the emission cone of duskside source regions under changing magnetospheric conditions such as the latitudinal extent of the aurora. To aid the interpretation of the AKR observations and disentangle the viewing and magnetospheric driving effects, we employ UV auroral observations from the DMSP/SSUSI instrument (Paxton et al., 1992; Carter et al., 2018).

The SSUSI instrument consists of a scanning spectrometer that observes the aurora in select wavelengths, capturing electron precipitation through their interaction with the ionosphere. As a DMSP spacecraft passes over the pole, taking ~ 20 minutes, observations of segments perpendicular to the footpath of the satellite are made. For this analysis, SSUSI observations of auroral radiance and the corresponding position in the oval are binned over 15 seconds and averaged to give values representing a relatively small local area. We use data from the DMSP F18 spacecraft and the LBHS channel (N2 emission, 140-150 nm). To discern the AKR origin from UV aurora, SSUSI observations of the dayside oval from each polar pass are subset into 4 hour wide magnetic local time (MLT) sectors. Given the slight variation in spacecraft trajectory for each orbit and subsequent spatial sampling, each MLT sector for each orbit has a differing number of data included, also varying between orbits. The sampling of SSUSI dictates that comparisons between the AKR and auroral emission cannot be quantified certainly on timescales less than approximately 40 minutes, so data in each sector are averaged. The time representing these averages is the median observation time of the orbital pass.

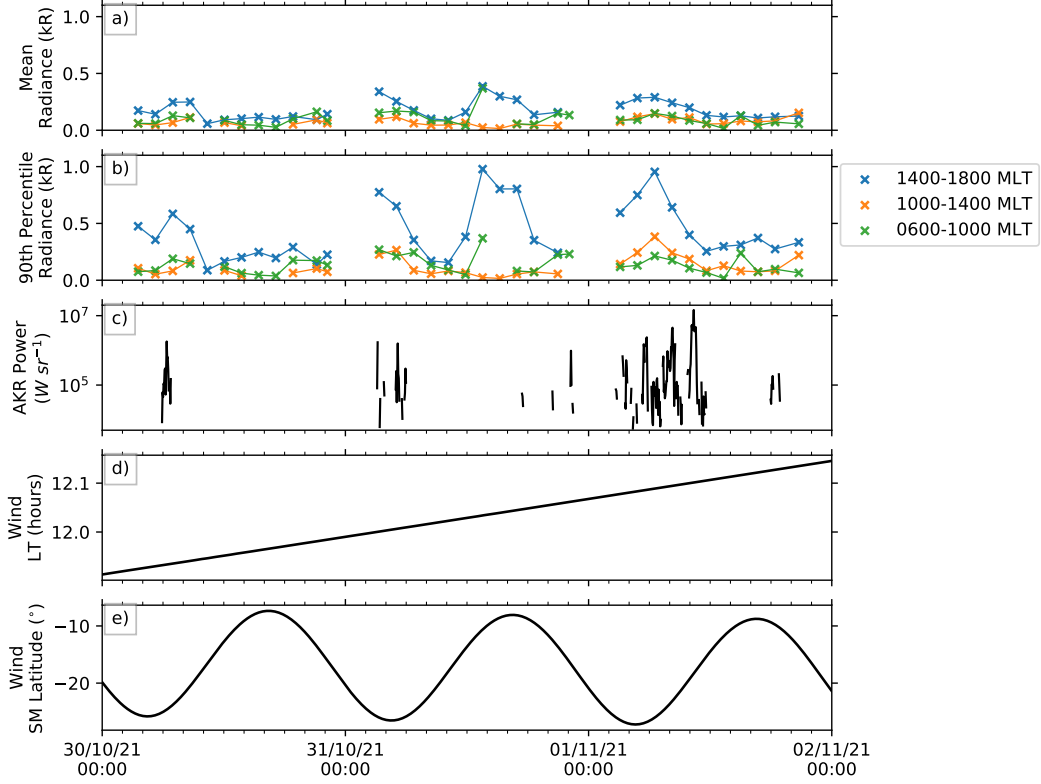


Figure 3. a) Mean and b) 90th percentile of electron auroral radiances for 4 hour wide MLT sectors on the dayside, with each marker representing selected DMSP/SSUSI observations. c) Fractional emitted AKR power from Wind/WAVES, integrated between 30-650 kHz. d) LT and e) latitude of Wind in the solar magnetic coordinate system.

Figure 3 shows the SSUSI observations of UV auroral radiance in kR, reduced over each orbit of the DMSP F18 spacecraft for this period and subset in MLT sectors 06:00-10:00, 10:00-14:00 and 14:00-18:00 hours. Panels a and b show the mean averaged and 90th percentile values of the auroral radiances for each MLT sector. Also shown is the AKR power (c), integrated between 30-650 kHz, and the LT (d) and latitude (e) of the Wind spacecraft in the geocentric solar ecliptic and solar magnetic (SM) coordinate systems, respectively. The latter show the slowly varying LT of Wind as it orbits L1, and the SM latitude varies as the magnetic dipole tilts with the diurnal rotation.

The afternoon sector (14:00-18:00 MLT) exhibits the brightest mean auroral radiance (Figure 3a) of the dayside for these observations, reaching the maximum of 0.39 kR at around 13:00 UT on 31st October 2021, the same time as the largest substorm onset here. Although peaks in auroral radiance with similar magnitude occur in the afternoon sector at other times in this 3 day period, the orbital pass centred closest to 13:00 UT also observes aurora in the morning sector that is uncommonly bright for these observations at 0.37 kR. Figure 3b shows the 90th percentile from each MLT sector, representing extreme occurrences and likely the presence of bright, discrete aurora for values much higher than the mean. This is true for the afternoon sector where peak 90th percentile values are between 2-3 times that of the mean. Extreme values in other MLT sectors exhibit similar values to the mean, suggesting either that their aurora is diffuse or that there are not many data observed in those sectors for those orbital passes.

The AKR observations are shown here in terms of the power in W sr^{-1} , and are derived directly from the flux density in Figure 2d. Observed AKR bursts for this period exhibit a peak power of $\sim 10^6 \text{ W sr}^{-1}$. The most powerful AKR burst, with a peak at $\sim 10:15$ UT, reaches $> 10^7 \text{ W sr}^{-1}$. The average AKR power observed by Wind between 1995-2004, and from LTs between 11:30-12:30, is between 5×10^4 and $6 \times 10^4 \text{ W sr}^{-1}$ (J. W. Waters et al., 2022). The median AKR power observed for this period from 12:00 LT is $6.4 \times 10^4 \text{ W sr}^{-1}$. With the exception of the peak in the auroral radiance at 13:00 UT on 31st October 2021, the bright, discrete auroral emissions in the afternoon sector are accompanied by AKR bursts.

As AKR source regions exist on high latitude magnetic field lines, they will tilt with the magnetic axis as Earth rotates. Figures 3c and 3e show that, generally, AKR is observed from L1 when Wind is furthest from the magnetic equator. This agrees with previous studies of the effect of the observer latitude on AKR viewing (Lamy et al., 2010; J. E. Waters et al., 2021), and is expected given the beaming from the source region (Mutel et al., 2008). This would also explain the lack of observed AKR during the strongest substorm onset of the period at 13:00 on 31st October 2021, with which the bright auroral radiance is associated.

However, with the remote sensing observations here, it is difficult to discern the true nature of the observations; while SSUSI observations exhibit auroral brightenings, the latitude, longitudinal extent and the auroral intensity below regions of strong upward FAC that would generate AKR could combine to influence the measurements. A statistical study of L1 observations and latitudinal effects is needed to properly discern between viewing effects or a lack of AKR bursting on the dayside. However, it is clear that the observed AKR power is related to bright auroral structures between 14:00-18:00 MLT. Previous mapping of AKR sources to discrete auroral structures (Huff et al., 1988; Menietti et al., 2011; Yearby & Pickett, 2022) and the presence of strong upward FACs required for their existence suggest this is the auroral source of the AKR. These structures are likely to be associated with the ionospheric current system that travels Westward at substorm onset, given the SML profile for this period. These AKR observations are thus the first to be made from L1 in a case study context, and are the first to show dayside AKR sources likely associated with substorm onset.

3 Summary

An ICME that erupted from the Sun on 28th October 2021 was accompanied by an X1.0 class solar flare and intense radio emissions, with SEPs producing GLEs measured at Earth. The associated magnetic structures rapidly induced an SSC geomagnetic storm when they reached Earth ~ 2 days later, revealed in the OMNI solar wind observations and the SYM-H geomagnetic index. Using derivative measures of solar wind parameters, namely the Milan et al. (2012) dayside reconnection rate, and of ground magnetometers in the PC and SuperMAG indices, we showed the subsequent transport of plasma across the magnetosphere and the resulting current dynamics, indicating the presence of substorm onset prior to and following the initial dynamic pressure enhancement at 19:00 on 30th October 2021.

Novel observations of AKR by Wind at L1 are presented, that show bursts that exceed the 10 year average from the same LT by 3 orders of magnitude. Bursts are observed when Wind is further from the magnetic equator, suggesting a longitudinal and latitudinal viewing effect. SSUSI auroral observations show discrete aurora in the afternoon sector that correlate with the bursts, and an occasion of diffuse aurora in the morning sector during AKR. This makes direct inference of a dayside AKR source uncertain but likely corresponds to the discrete aurora for this period, which also correlates with nightside substorm activity. While L1 observations are useful when comprehensive conjugate observations are available, more work is needed to supplement usual proxies of magnetospheric disturbance with remote Wind/WAVES radio measurements of AKR from L1.

Acknowledgments

J. E. Waters’s work was supported by the EPSRC Centre for Doctoral Training in Next Generation Computational Modelling Grant No. EP/L015382/1.

C.M.J. and A.R.F.’s work is supported by the Science Foundation Ireland Grant 18/FRL/6199

We acknowledge use of NASA/GSFC’s Space Physics Data Facility’s OMNIWeb service, and OMNI data.

We gratefully acknowledge the SuperMAG collaborators (<https://supermag.jhuapl.edu/info/?page=acknowledgement>).

The authors acknowledge CNES (Centre National d’Etudes Spatiales), CNRS (Centre National de la Recherche Scientifique), and Observatoire de Paris for support to the Wind/Waves team and the CDPP (Centre de Données de la Physique des Plasmas) for the provision of the Wind/Waves RAD1 L2 data. The authors acknowledge support from Paris Astronomical Data Centre (PADC) for the preparation and distribution of the data collection.

The AKR-selected data from Wind/WAVES can be accessed online at the following link: <https://doi.org/10.25935/wxv0-vr90>

OMNI data including IMF B_Y and B_Z , V_{SW} , N_{SW} , P_{SW} and SYM-H indices were obtained via OMNIWeb (<https://omniweb.gsfc.nasa.gov/hw.html>).

Preliminary PC(N/S) indices were provided by World Data Center for Geomagnetism, Copenhagen and obtained from <https://pcindex.org/archive?>.

SSUSI data were obtained from <https://ssusi.jhuapl.edu/>.

References

- Alexander, J. K., & Kaiser, M. L. (1976, dec). Terrestrial kilometric radiation, 1. Spatial structure studies. *Journal of Geophysical Research*, 81(34), 5948–5956. Retrieved from <http://doi.wiley.com/10.1029/JA081i034p05948> doi: 10.1029/JA081i034p05948
- Alexander, J. K., & Kaiser, M. L. (1977, jan). Terrestrial kilometric radiation, 2. Emission from the magnetospheric cusp and dayside magnetosheath. *Journal of Geophysical Research*, 82(1), 98–104. Retrieved from <http://doi.wiley.com/10.1029/JA082i001p00098> doi: 10.1029/JA082i001p00098
- Araki, T. (1994, jan). A Physical Model of the Geomagnetic Sudden Commencement. In M. J. Engebretson, K. Takahashi, & M. Scholer (Eds.), (pp. 183–200). Washington, D. C.: American Geophysical Union. Retrieved from <http://doi.wiley.com/10.1029/GM081p0183> <http://doi.wiley.com/10.1029/GM081> doi: 10.1029/GM081
- Brueckner, G. E., Howard, R. A., Koomen, M. J., Korendyke, C. M., Michels, D. J., Moses, J. D., ... Eyles, C. J. (1995, dec). The Large Angle Spectroscopic Coronagraph (LASCO). *Solar Physics*, 162(1-2), 357–402. Retrieved from <http://link.springer.com/10.1007/BF00733434> doi: 10.1007/BF00733434
- Carter, J. A., Milan, S. E., Fogg, A. R., Paxton, L. J., & Anderson, B. J. (2018). The Association of High-Latitude Dayside Aurora With NBZ Field-Aligned Currents. *Journal of Geophysical Research: Space Physics*, 123(5), 3637–3645. doi: 10.1029/2017JA025082
- Carter, J. A., Milan, S. E., Fogg, A. R., Sangha, H., Lester, M., Paxton, L. J., & Anderson, B. J. (2020). The Evolution of Long-Duration Cusp Spot Emission During Lobe Reconnection With Respect to Field-Aligned Currents. *Journal of Geophysical Research: Space Physics*, 125(7). doi: 10.1029/2020JA027922
- Coxon, J. C., Milan, S. E., Clausen, L. B., Anderson, B. J., & Korth, H. (2014). A superposed epoch analysis of the regions 1 and 2 Birkeland currents observed by AMPERE during substorms. *Journal of Geophysical Research: Space Physics*, 119(12), 9834–9846. doi: 10.1002/2014JA020500
- Davis, T. N., & Sugiura, M. (1966, feb). Auroral electrojet activity index AE and its universal time variations. *Journal of Geophysical Research*, 71(3), 785–801. Retrieved from <http://doi.wiley.com/10.1029/JZ071i003p00785> doi: 10.1029/JZ071i003p00785
- Fogg, A. R., Jackman, C. M., Waters, J. E., Bonnin, X., Lamy, L., & Cecconi, B. (2022). Wind / WAVES observations of Auroral Kilometric Radiation : automated burst detection and Terrestrial Solar Wind - Magnetosphere coupling effects. *Journal of Geophysical Research: Space Physics*, 1–28.
- Forsyth, C., Rae, I. J., Coxon, J. C., Freeman, M. P., Jackman, C. M., Gjerloev, J., & Fazakerley, A. N. (2015, dec). A new technique for determining Substorm Onsets and Phases from Indices of the Electrojet (SOPHIE). *Journal of Geophysical Research: Space Physics*, 120(12), 10,592–10,606. Retrieved from <http://doi.wiley.com/10.1002/2015JA021343> doi: 10.1002/2015JA021343
- Gjerloev, J. W. (2012). The SuperMAG data processing technique. *Journal of Geophysical Research: Space Physics*, 117(9), 1–19. doi: 10.1029/2012JA017683
- Gurnett, D. A. (1974, oct). The Earth as a radio source: Terrestrial kilometric radiation. *Journal of Geophysical Research*, 79(28), 4227–4238. Retrieved from <http://doi.wiley.com/10.1029/JA079i028p04227> doi: 10.1029/JA079i028p04227
- Hanasz, J., Boudjada, M. Y., Schreiber, R., Krawczyk, Z., Malycha, M., Mogilevsky, M. M., ... Romantsova, T. V. (2000, jun). Dynamic spectra of the Stokes parameters for the dayside and nightside auroral kilometric radiation. *Geophysical Research Letters*, 27(11), 1631–1634. Retrieved from <http://>

- doi.wiley.com/10.1029/1999GL010770 doi: 10.1029/1999GL010770
- Huff, R. L., Calvert, W., Craven, J. D., Frank, L. A., & Gurnett, D. A. (1988, oct). Mapping of auroral kilometric radiation sources to the aurora. *Journal of Geophysical Research*, 93(A10), 11445. Retrieved from <http://doi.wiley.com/10.1029/JA093iA10p11445> doi: 10.1029/JA093iA10p11445
- Hutchinson, J. A., Wright, D. M., & Milan, S. E. (2011). Geomagnetic storms over the last solar cycle: A superposed epoch analysis. *Journal of Geophysical Research: Space Physics*, 116(9), 1–16. doi: 10.1029/2011JA016463
- Iyemori, T. (1990). Storm-time magnetospheric currents inferred from mid-latitude geomagnetic field variations. *Journal of geomagnetism and geoelectricity*, 42(11), 1249–1265. Retrieved from <http://www.jstage.jst.go.jp/article/jgg1949/42/11/42{\-}11{\-}1249/{\-}article> doi: 10.5636/jgg.42.1249
- Kilpua, E. K., Balogh, A., von Steiger, R., & Liu, Y. D. (2017). Geoeffective Properties of Solar Transients and Stream Interaction Regions. *Space Science Reviews*, 212(3-4), 1271–1314. Retrieved from <http://dx.doi.org/10.1007/s11214-017-0411-3> doi: 10.1007/s11214-017-0411-3
- Klein, K.-L., Musset, S., Vilmer, N., Krucker, S., Battaglia, A., Dresing, N., & Palmroos, C. (2022). [in prep] The relativistic solar particle event on 28 October 2021: evidence on particle acceleration in and escape from the solar corona. *Astronomy and Astrophysics*.
- Lamy, L., Zarka, P., Cecconi, B., & Prangé, R. (2010, sep). Auroral kilometric radiation diurnal, semidiurnal, and shorter-term modulations disentangled by Cassini. *Journal of Geophysical Research: Space Physics*, 115(A9), n/a–n/a. Retrieved from <http://doi.wiley.com/10.1029/2010JA015434> doi: 10.1029/2010JA015434
- Menietti, J. D., Mutel, R. L., Christopher, I. W., Hutchinson, K. A., & Sigwarth, J. B. (2011). Simultaneous radio and optical observations of auroral structures: Implications for AKR beaming. *Journal of Geophysical Research: Space Physics*, 116(12), 1–9. doi: 10.1029/2011JA017168
- Milan, S. E., Gosling, J. S., & Hubert, B. (2012, mar). Relationship between interplanetary parameters and the magnetopause reconnection rate quantified from observations of the expanding polar cap. *Journal of Geophysical Research: Space Physics*, 117(A3), n/a–n/a. Retrieved from <http://doi.wiley.com/10.1029/2011JA017082> doi: 10.1029/2011JA017082
- Morioka, A., Miyoshi, Y., Kurita, S., Kasaba, Y., Angelopoulos, V., Misawa, H., ... McFadden, J. P. (2013). Universal time control of AKR: Earth is a spin-modulated variable radio source. *Journal of Geophysical Research: Space Physics*, 118(3), 1123–1131. doi: 10.1002/jgra.50180
- Morioka, A., Miyoshi, Y., Tsuchiya, F., Misawa, H., Sakanoi, T., Yumoto, K., ... Donovan, E. F. (2007). Dual structure of auroral acceleration regions at substorm onsets as derived from auroral kilometric radiation spectra. *Journal of Geophysical Research: Space Physics*, 112(6), 1–13. doi: 10.1029/2006JA012186
- Mutel, R. L., Christopher, I. W., & Pickett, J. S. (2008, apr). Cluster multispacecraft determination of AKR angular beaming. *Geophysical Research Letters*, 35(7), n/a–n/a. Retrieved from <http://doi.wiley.com/10.1029/2008GL033377> doi: 10.1029/2008GL033377
- Mutel, R. L., Gurnett, D. A., & Christopher, I. W. (2004). Spatial and temporal properties of AKR burst emission derived from Cluster WBD VLBI studies. *Annales Geophysicae*, 22(7), 2625–2632. doi: 10.5194/angeo-22-2625-2004
- Newell, P. T., & Gjerloev, J. W. (2011, dec). Evaluation of SuperMAG auroral electrojet indices as indicators of substorms and auroral power. *Journal of Geophysical Research: Space Physics*, 116(A12), n/a–n/a. Retrieved from <http://doi.wiley.com/10.1029/2011JA016779> doi: 10.1029/2011JA016779
- Nishimura, Y., Lyons, L. R., Gabrielse, C., Sivadas, N., Donovan, E. F., Varney,

- R. H., ... Zhang, S. R. (2020). Extreme Magnetosphere-Ionosphere-Thermosphere Responses to the 5 April 2010 Supersubstorm. *Journal of Geophysical Research: Space Physics*, 125(4), 1–15. Retrieved from <https://doi.org/10.1029/2019JA027654> doi: 10.1029/2019JA027654
- Papaioannou, A., Kouloumvakos, A., Mishev, A., Vainio, R., Usoskin, I., Herbst, K., ... Kühl, P. (2022, feb). The First Ground Level Enhancement of Solar Cycle 25 on 28 October 2021. *Astronomy and Astrophysics*, 71(September 2017), 1–9. Retrieved from <http://arxiv.org/abs/2202.07927>
- Paxton, L. J., Meng, C.-I., Fountain, G. H., Ogorzalek, B. S., Darlington, E. H., Gary, S. A., ... Smith, B. E. (1992). Special Sensor Ultraviolet Spectrographic Imager: An Instrument Description. *Instrumentation for Planetary and Terrestrial Atmospheric Remote Sensing*, 1745(June 1992), 2–15. doi: 10.1117/12.60595
- Pedersen, B. M., Pottelette, R., Eliasson, L., Murphree, J. S., Elphinstone, R. D., Bahnsen, A., & Jespersen, M. (1992). Auroral kilometric radiation from transpolar arcs. *Journal of Geophysical Research*, 97(A7), 10567. Retrieved from <http://doi.wiley.com/10.1029/92JA00410> doi: 10.1029/92JA00410
- Stauning, P. (2013). The Polar Cap index: A critical review of methods and a new approach. *Journal of Geophysical Research: Space Physics*, 118(8), 5021–5038. doi: 10.1002/jgra.50462
- Taylor, J. R., Lester, M., & Yeoman, T. K. (1994, jun). A superposed epoch analysis of geomagnetic storms. *Annales Geophysicae*, 12(7), 612–624. Retrieved from <https://angeo.copernicus.org/articles/12/612/1994/> doi: 10.1007/s00585-994-0612-4
- Treumann, R. A. (2006). The electron-cyclotron maser for astrophysical application. *Astronomy and Astrophysics Review*, 13(4), 229–315. doi: 10.1007/s00159-006-0001-y
- Troshichev, O. A., & Andrezen, V. G. (1985). The relationship between interplanetary quantities and magnetic activity in the southern polar cap. *Planetary and Space Science*, 33(4), 415–419. doi: 10.1016/0032-0633(85)90086-8
- Walach, M. T., & Grocott, A. (2019). SuperDARN Observations During Geomagnetic Storms, Geomagnetically Active Times, and Enhanced Solar Wind Driving. *Journal of Geophysical Research: Space Physics*, 124(7), 5828–5847. doi: 10.1029/2019JA026816
- Waters, J. E., Jackman, C. M., Lamy, L., Cecconi, B., Whiter, D. K., Bonnin, X., ... Fogg, A. R. (2021, oct). Empirical Selection of Auroral Kilometric Radiation During a Multipoint Remote Observation With Wind and Cassini. *Journal of Geophysical Research: Space Physics*, 126(10), 1–26. Retrieved from <https://onlinelibrary.wiley.com/doi/10.1029/2021JA029425> doi: 10.1029/2021JA029425
- Waters, J. W., Jackman, C. M., Whiter, D. K., Forsyth, C., Fogg, A. R., Lamy, L., ... Issautier, K. (2022). [submitted] A perspective on substorm dynamics using 10 years of Auroral Kilometric Radiation observations from Wind. *Journal of Geophysical Research: Space Physics*. doi: 10.1002/essoar.10510871.1
- Wu, C. S., & Lee, L. C. (1979). A theory of the terrestrial kilometric radiation. *The Astrophysical Journal*, 230, 621. Retrieved from <http://adsabs.harvard.edu/doi/10.1086/157120> doi: 10.1086/157120
- Yearby, K. H., & Pickett, J. S. (2022, feb). A Review of Cluster Wideband Data Multi-Spacecraft Observations of Auroral Kilometric Radiation. *Journal of Geophysical Research: Space Physics*, 127(2). Retrieved from <https://onlinelibrary.wiley.com/doi/10.1029/2021JA029499> doi: 10.1029/2021JA029499
- Zhao, W., Liu, S., Zhang, S., Zhou, Q., Yang, C., He, Y., ... Xiao, F. (2019). Global Occurrences of Auroral Kilometric Radiation Related to Suprathermal Electrons in Radiation Belts. *Geophysical Research Letters*, 2, 7230–7236. doi:

